An Efficient RF Exposure System with Precise Whole-Body Average SAR Determination for *in vivo* Animal Studies at 900 MHz

Quirino Balzano, *Senior Member, IEEE*, Chung-Kwang Chou, *Fellow, IEEE*, Renato Cicchetti, *Member, IEEE*, Antonio Faraone, *Member, IEEE*, and Roger Yew-Siow Tay, *Member, IEEE*

***Abstract*—A radial electromagnetic cavity has been designed and optimized for the *in vivo* whole-body exposure of mice to 900-MHz RF fields. Parallel circular plates shorted around the perimeter form the cavity, which is fed at the center in order to excite a cylindrical TEM wave. Plastic housings allow the insertion and equidistant positioning from the exciter of 40 mice, with the electric field parallel to the body axis. The resulting exposure system is highly efficient, featuring more than 80% of the incident power dissipated in the mice. The whole-body average SAR can be determined with remarkable precision by means of straightforward power balance since the RF power leakage from the cavity is extremely low. Fairly uniform exposure of the mice, individually and collectively, has been achieved by means of the symmetric arrangement. This exposure system has been adopted in a replication study on transgenic mice currently being carried out in South Australia, and is being considered for upcoming animal studies in Europe.**

***Index Terms*—Animal exposure, bioassay, radial cavity, RF dosimetry, SAR.**

I. Introduction

POTENTIAL biological effects of nonionizing radiation can be investigated by carrying out long-term animal exposure studies [1]–[6]. Depending on the particular effect under investigation, choice of the animals can vary from primates to rodents. In order to isolate possible frequency, modulation, or dose-dependent effects, different signals and exposure levels can be chosen. Electromagnetic exposure to RF sources is quantified in terms of the specific absorption rate (SAR), i.e., the time rate of electromagnetic energy deposition per unit mass: $SAR = \sigma|\mathbf{E}|^2/\rho$, σ being the equivalent conductivity of the medium, ρ the density, and $|\mathbf{E}|$ the rms electric field strength [7]. On the basis of established scientific evidence, present safety guidelines prescribe whole-body averaged and localized (1- or 10-g averages) SAR limits [8], [9]. Hence, depending on the target of a particular study, the animal exposure can be systemic or specific to a particular organ, e.g., brain. The choice of the exposure system and the use of appropriate dosimetric techniques must ensure the delivery of specific SAR levels that are quantifiable throughout the study, which can last as long as two years for rodents.

Whole-body animal exposure to (locally) plane waves has been accomplished in the past by means of circular or rectangular waveguides, radial waveguides, and rectangular horns, e.g., those described in [10]–[13]. The reader will find the relevant bibliography in [14]. In these structures, the matching of the antenna to the RF source is fairly insensitive of the loading, e.g., animal orientation with respect to the incident field. Electromagnetic cavities have seldom been employed since tuning is very sensitive to load changes, forcing posture constraints of the animals, with the consequence of imposing restrictions on maximum exposure duration to avoid excessive stress. However, whenever a constrained exposure is possible, cavities allow a precise determination of the whole-body averaged SAR in the animals, as well as an efficient use of the available RF power.

In this paper, we present the design of an exposure system presently employed in a long-term study on mice exposed to GSM-modulated fields at 900 MHz, which is the replication of a study performed using completely different exposure conditions [3]. The system has a wider range of application, though, as it can be employed in long-term mice studies wherever the RF exposure is nonlocalized and the daily exposure is limited to a few hours.

The structure of this paper is as follows. In Section II, we discuss the design requirements for the exposure system, while in Section III, the actual design is illustrated. Section IV describes the techniques employed to determine the whole-body average SAR in the mice. In Section V, we further discuss some particular features of the exposure system and illustrate future developments, while the conclusions are drawn in Section VI.

II. "Ferris-Wheel" Mice Exposure System

The purpose of this project is to design a mice exposure system for an Australian *in vivo* study on transgenic mice exposed to the global system of mobile communication (GSM) 900-MHz signal. The most important design requirements are: 1) plane-wave-like incident fields, with excellent individual and collective uniformity of animal exposure and 2) precisely quantifiable whole-body average SAR, the target levels being 4, 2, 1, 0.25, and 0 W/kg (sham exposed) for different mice populations. Strong consideration is given to the available space in the exposure facility at the Institute of Medical and Veterinary Science (IMVS), Adelaide, South Australia. Addi-

Manuscript received November 10, 1999; revised February 28, 2000.

Q. Balzano, C.-K. Chou, and A. Faraone are with the Motorola Florida Research Laboratories, Fort Lauderdale, FL 33322 USA.

R. Cicchetti is with the Department of Electronic Engineering, University of Rome "La Sapienza" I-00184 Rome, Italy.

R. Y.-S. Tay is with the Singapore Design Center, Motorola Electronics Pte. Ltd, Singapore.

Publisher Item Identifier S 0018-9480(00)09695-2.

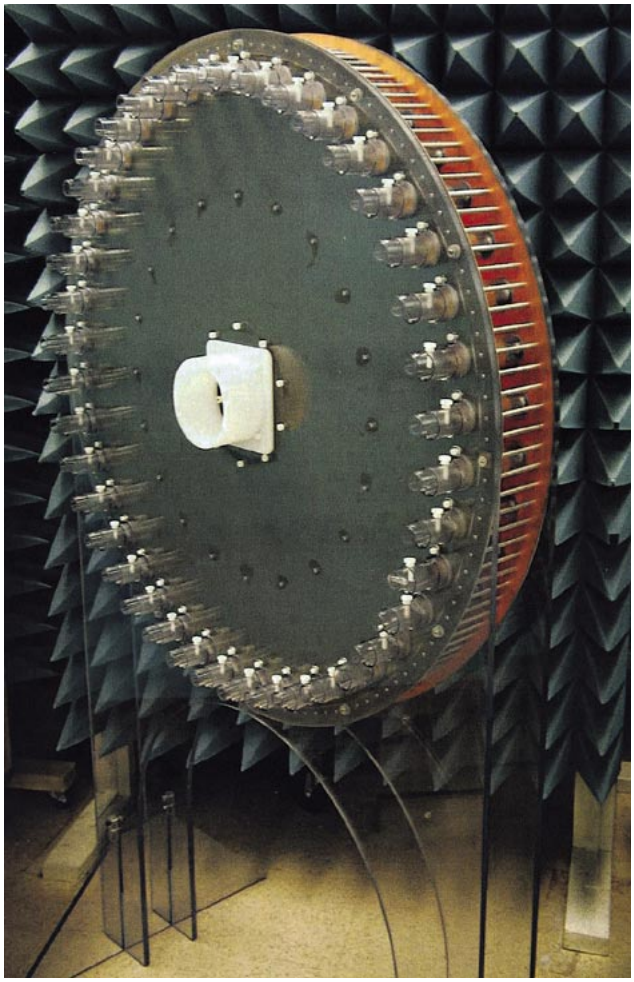

Fig. 1. "Ferris-wheel" exposure system for mice.

tional constraints derive from the large number of exposed mice (1200) and exposure duration (1-h daily per mouse population), as well as the cost of the RF equipment (with the consequent limitation to about 25-W average RF power available per exposure unit).

The outcome is the exposure system, as shown in Fig. 1, nicknamed the "Ferris wheel" for its appearance. The exposure system comprises a radial electromagnetic cavity formed by parallel circular plates mounted on a polycarbonate frame, joined around the perimeter by an array of shorting posts. A tunable transition from a 50-Ω coaxial feed line excites a cylindrical TEM wave that impinges on a carousel of 40 symmetrically arranged mice, which are equidistant from the exciter. The mice, restrained in plastic tubes inserted through circular holes in the plates, as shown in Fig. 2, are held co-polarized with the incident electric field (E-polarization) to maximize the absorption of RF energy. Proper ventilation is provided to the animals by a dc-motor driven fan. The symmetric arrangement provides uniform exposure to the mice, while the whole-body TEM illumination induces fairly uniform RF absorption within each mouse. Depending on the position of a mouse in the carousel, the wave impinges from different directions. Therefore, the mice are rotated on a daily basis to achieve as uniform absorption as possible throughout the chronic exposure.

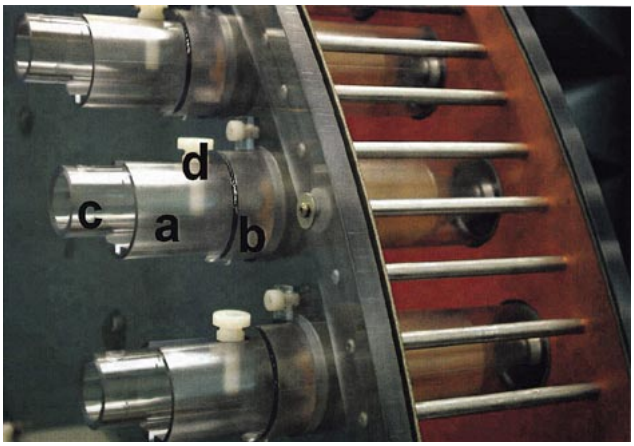

Fig. 2. Mouse restraining mechanism. (a) The mouse holder that slides and locks to (b) the plastic sleeve attached to the cavity frame. (c) A pusher is held to the restrainer by means of (d) the thumbscrew to keep the mouse exposed inside the "Ferris wheel."

The previously mentioned design constraints led us to assign 40 mice per exposure unit. Fifteen units equally split in the five 2.6 m $\times$ 4.5 m exposure rooms would allow the simultaneous exposure of 600 mice, meaning that two shifts (morning and afternoon) would be sufficient to expose all mice populations. As the mass of adult female mice typically ranges from 25 to 30 g, 4–5 W need to be dissipated in each exposure unit to achieve the maximum whole-body SAR level of 4 W/kg. Anticipating a 2-dB pathloss due to RF cables and the bidirectional coupler, only about 16 W out of the 25 W provided by the amplifier would be available at the cavity feed point. The ensuing 25%–30% minimum efficiency requirement would not be trivial to achieve in electromagnetically open exposure systems. The "Ferris-wheel" cavity achieves about 80%. In the following sections, many of the aspects just mentioned will be addressed in more detail as we illustrate the design of this exposure system.

A. Discussion

A radial waveguide [15] would be a convenient structure to provide uniform collective illumination of numerous bodies symmetrically disposed. Locally, the incident field is a free-space-like TEM plane wave, as long as circumferential or longitudinal higher order mode excitation is not very significant. Assuming the cylindrical reference frame $\{\rho, \phi, z\}$ in Fig. 3, the field components are (see the Appendix)

$$E_z(\rho) = A_r H_0^{(1)}(k\rho) + A_f H_0^{(2)}(k\rho) \tag{1}$$

$$H_\phi(\rho) = \frac{1}{-j\eta}\left[A_r H_1^{(1)}(k\rho) + A_f H_1^{(2)}(k\rho)\right] \tag{2}$$

where k is the wavenumber and η is the wave impedance in the medium. Already at a short distance ($\rho > \lambda/2$), the cylindrical wave impedance approaches the plane-wave impedance, i.e., $E_z(\rho)/H_\phi(\rho) \approx \eta$ for progressive waves ($A_r = 0$). Therefore, an exposure in the radial waveguide is very similar to free space, provided the $\rho - \phi$ cross section of the exposed body is much smaller than its distance from the center so that the impinging wavefront can be considered locally flat and uniform. The advantage is the compactness in terms of volume to number

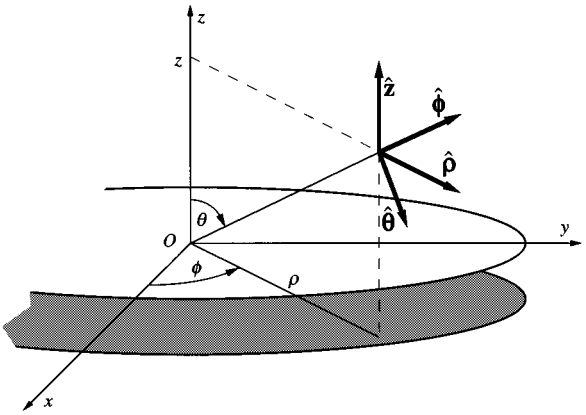

Fig. 3. Reference frames associated with the radial cavity.

of exposed animals, when compared to other whole-body exposure systems such as waveguides, exposure chambers (shielded, anechoic, or semianechoic), or large horn antennas.

Some distinct advantages derive from terminating a radial waveguide on a matched load, e.g., RF absorbers placed around the perimeter. Good impedance matching to the RF source is typically broad-band and, to some extent, insensitive to the position and size of the exposed bodies. On the other hand, power efficiency can be relatively low as a considerable share of the impinging energy may bypass the animals and dissipate in the absorbers. Given the impossibility to measure such dissipation, the whole-body SAR must be determined for many animal sizes and postures, using calorimetric or numerical techniques having substantial intrinsic uncertainty.

A shorting electric wall around the circular perimeter converts the radial waveguide into a cavity. The mice can be placed equidistant from its center and from each other to symmetrically load the cavity. To maximize the RF absorption, the mice are E-polarized. Compared with the terminated waveguide, impedance matching is more sensitive to the cavity load, e.g., the mouse size. Moreover, the loaded cavity stores higher reactive energy so that a good impedance matching to the source is typically narrow-band. In light of this, a tunable coax-to-cavity transition is needed to enable good matching at the desired operating frequency. Typical solutions are reactive matching circuits such as single, double, or triple stub tuners (so-called "trombone lines"), which are external to the cavity and relatively encumbering, thus, we devised an internal transition with broad-band tuning ability. The distance of the mice from the lateral cavity walls turns out to be the most important efficiency-related parameter, which has been optimized by means of a simplified loaded-cavity model. The radial cavity allows a precise determination of the power dissipated inside by means of bidirectional power measurements, provided radiation losses are known. Moreover, the collective whole-body SAR in the mice can be easily monitored during the course of the study by collecting forward and reverse power data.

III. Design of the "Ferris Wheel"

Two circular single-side copper-clad laminate printed circuit boards (PCBs), separated by a 10-cm-long hollow Teflon cylinder about 10 cm in radius and 1.8-cm thick, are joined around the perimeter by an array of shorting posts to form the radial cavity. Forty mice are placed 9° apart at 44 cm from the center, E-polarized with respect to the incident TEM wave. Typically, female mice can weigh up to 30 g, thus, for the experimental design, we employed dummy equivalents, consisting of 30-cm^3 plastic bottles filled with tissue simulating mixture (water : sugar : salt : hydroxyethylcellulose ~53.5 : 44.25 : 1.15 : 1 weight-wise [16]). At 900 MHz, the mixture dielectric properties are: $\varepsilon_r \approx 51$, $\sigma \approx 1$ S/m. The cavity is fed at the center by an internal tunable transition from the coaxial feed line, which will be described later.

The dummies are inserted through circular apertures realized on both plates of the cavity. The aperture diameter is about 4 cm since it has to allow the insertion of plastic mouse holders on one side and insertion of ventilation hoses on the other. Minimal RF leakage is expected at 900 MHz, the corresponding wavelength being more than twice the aperture circumference, thus resulting in very low radiation efficiency.

An array of 120 shorting posts is preferred to a solid electric wall since it lets light into the cavity, which is needed by the mice. The posts are 10-cm long and 6.35-mm in diameter. They are symmetrically distributed around the perimeter of the cavity at 48 cm from the center, co-polarized with the electric field of the impinging TEM wave, and less than one-tenth of a wavelength apart to ensure low RF leakage. Return-loss measurements of the unloaded cavity showed that appreciable radiation would not result, which was confirmed by radiation measurements of the loaded cavity.

A. Tunable Coax-to-Radial Cavity Transition

Tuning ability of the cavity exciter is desired to ensure proper matching to the RF source over a relatively wide range of possible loading conditions. We designed a tunable transition from the coaxial feed line to the radial cavity with the objective of maximizing the modal conversion to the fundamental cavity mode by keeping the exciter's current as uniform as possible. As depicted in Fig. 4, the transition is formed by a top-loaded monopole antenna [17], which is capacitively coupled with a passive counterpoise. In this way, the accumulation of electric charges is concentrated in the small region comprising the capacitive loads so that the current along the monopole as well as the counterpoise is kept fairly uniform. Tuning of the loaded cavity is performed through adjusting the capacitive coupling by moving the counterpoise closer or farther from the monopole, which is easily accomplished by threads on its arm. A plastic counter-nut ensures good electrical contact of the counterpoise with the cavity plate. Pictorial details of the actual implementation of the tuning element are provided in Fig. 5.

At first, the tuning ability of this transition was demonstrated for a matched radial waveguide, formed by terminating the circular plates on wedge RF absorbers. In Fig. 6, the measured return-loss response shows the remarkable tuning capability that can be achieved over a wide frequency range. The dimensions used in this case are $h = 10$ cm, $h_1 = 48$ mm, $d_1 = 10$ mm, and $d_2 = 20$ mm. The main reason of choosing $d_2 > d_1$ is to allow some tolerance against axial misalignment of the counterpoise

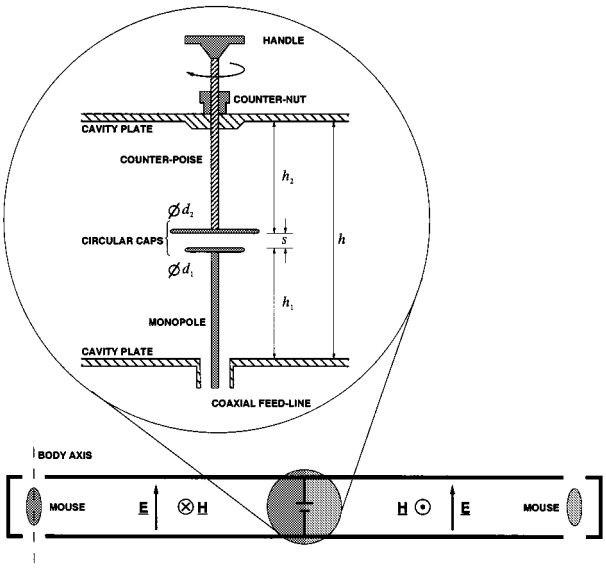

Fig. 4. Sketch of the tunable transition from the coaxial feed line to the radial cavity.

with respect to the monopole, so that the capacitive coupling between them is not substantially affected.

In the following section, after illustrating the optimization of the exposure system efficiency, the broad-band tuning ability will be demonstrated for the loaded radial cavity.

B. Efficiency Optimization of the Exposure System

As previously remarked, we found that the distance of the lateral wall from the mice is the principal parameter to optimize the efficiency of the exposure system. We employed a loaded-cavity model to come up with an initial estimate, replacing the 40 loads with a uniform lossy ring having the effective dielectric characteristics corresponding to the air-loads volumetric weighed average ($\varepsilon_t \approx 15, \sigma \approx 0.28$ S/m). The ring is 2.5-cm thick, the same as the diameter of the dummies, its minimum and maximum radii being 42.75 and 45.25 cm, respectively. The weighed average derives from the volumetric ratio between the ring and the 40 dummies, resulting in a scaling factor ≈0.28. In the real cavity, the distance between mice is less than a quarter-wavelength and, therefore, the approximation of a uniform loading ring is reasonable, as confirmed by the return-loss measurements. The cavity and its equivalent model are shown in Fig. 7. In each region, the cylindrical wave is expressed as

$$E_z^{(\nu)}(\rho) = A_r^{(\nu)} H_0^{(1)}(k_\nu \rho) + A_f^{(\nu)} H_0^{(2)}(k_\nu \rho), \quad \nu = 0, \cdots, 4 \tag{3}$$

$$H_\phi^{(\nu)}(\rho) = \frac{j}{\eta_\nu}\left[A_r^{(\nu)} H_1^{(1)}(k_\nu \rho) + A_f^{(\nu)} H_1^{(2)}(k_\nu \rho)\right], \quad \nu = 0, \cdots, 4 \tag{4}$$

provided η_ν, k_ν are those in the respective regions ($\varepsilon_r \approx 2.1$, no loss, assumed for Teflon). The solution of the linear system derived by enforcing the boundary conditions at the source, interfaces, and lateral cavity wall yields the unknowns $A_{f,r}^{(\nu)}$.

The dissipated power is given by the difference between forward and reverse real power at any distance closer than the lossy

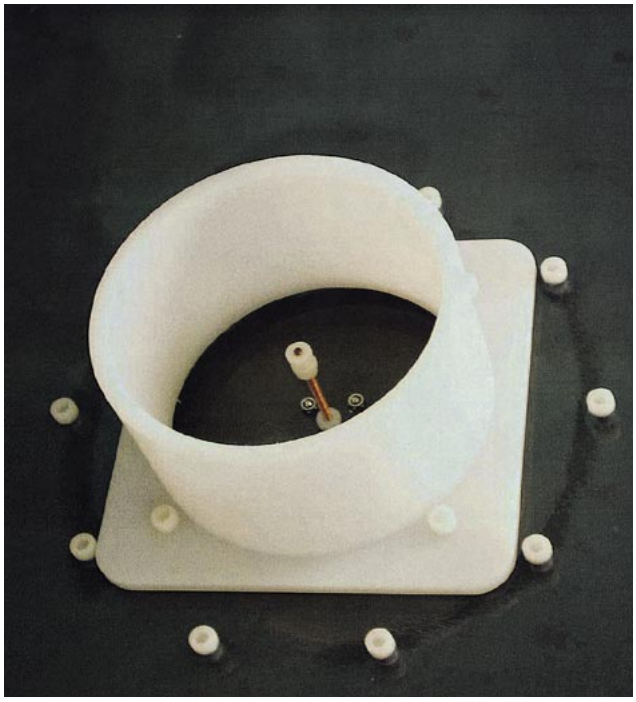

(a)

(b)

Fig. 5. Tunable transition. (a) Tuner handle with hollow Teflon cylinder (cap not shown) protecting from inadvertent crash. (b) Tuning element with mechanical support.

ring. The ratio of these quantities is independent of the actual power delivered

$$\frac{P_r}{P_f} = -\frac{|A_f^{(\nu)}|^2 \mathrm{Re}\left\{H_0^{(2)}(k_\nu \rho) H_1^{(2)}(k_\nu \rho)^* / j\eta_\nu\right\}}{|A_r^{(\nu)}|^2 \mathrm{Re}\left\{H_0^{(1)}(k_\nu \rho) H_1^{(1)}(k_\nu \rho)^* / j\eta_\nu\right\}}, \quad \nu < 3 \tag{5}$$

thus, it allows to establish the optimal distance between the load and lateral cavity wall. In Fig. 8, a parametric study performed at 900 MHz shows that sharp changes in (5) result from varying the distance of the mice from the cavity's lateral wall. The periodic dependence indicates that the best matching is achieved when the short-circuited radial waveguide section acts as an inductive load, against the common guess that best absorption would occur at the peak of the electric field at about a quarter-wave

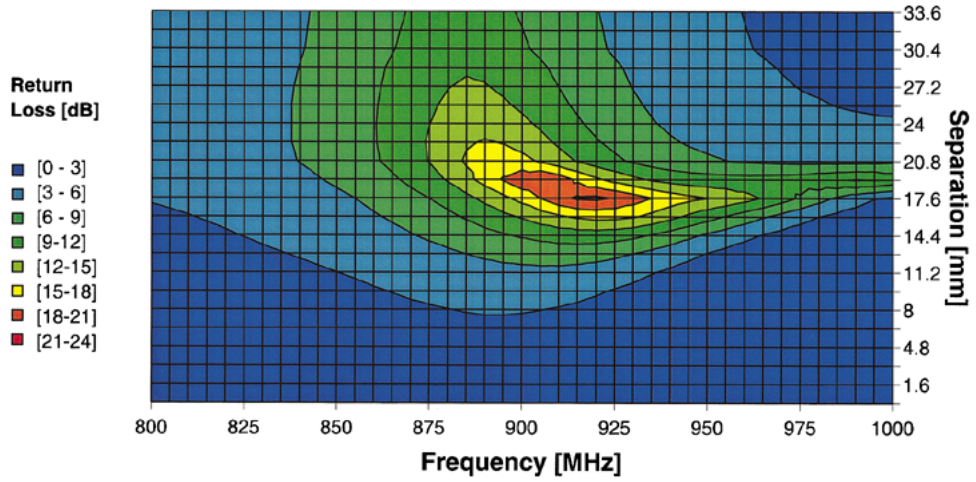

Fig. 6. Return loss of the radial waveguide obtained by terminating the cavity on absorbers, achieved by using the tunable exciter to optimize the impedance match to 50 Ω.

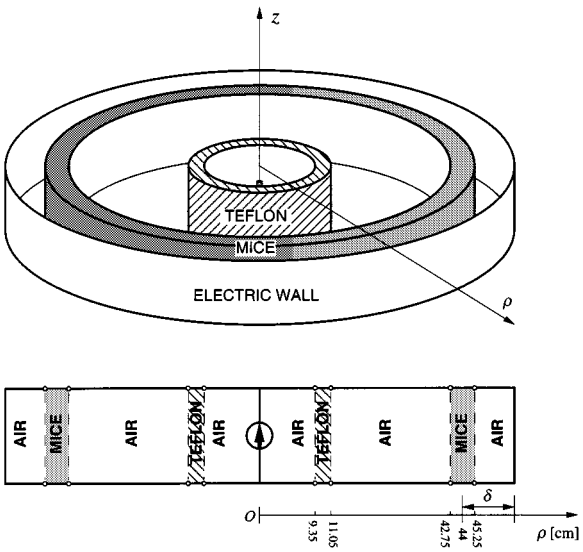

Fig. 7. Radial transmission-line model of the exposure system used to optimize the geometry.

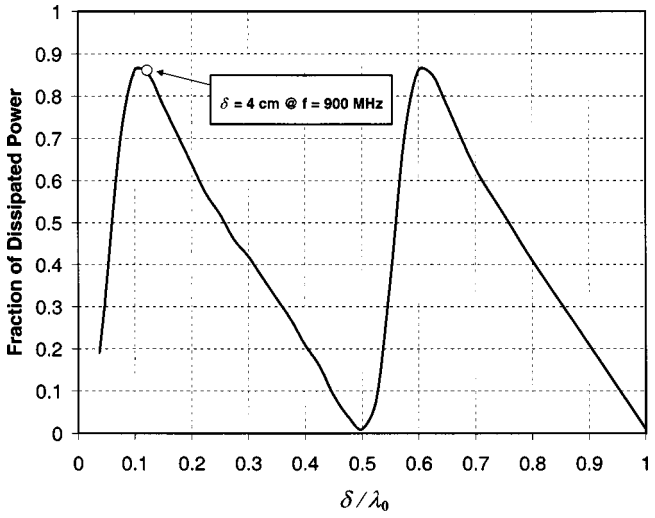

Fig. 8. Fraction of the incident RF power that is dissipated in the mice versus distance of the shorting wall, according to the radial-transmission-line model. The optimal distance is pointed out.

from the short. Evidently, the nature of the lossy load is not purely resistive and, therefore, the dissipation of RF power is maximized under particular reactive loading conditions, which are inductive in nature in this particular case. Moreover, additional phase delay occurs due to the distributed nature of the load and its dielectric characteristics.

An excellent agreement resulted from experimental checks of the theoretical predictions. A prototype of the cavity was built, where the shorting posts could be placed at five different distances from 48 to 50 cm. On the base of return loss and thermometric measurements (the latter will be described later), the optimal distance was found at 48 cm from the center (4 cm from the mouse body axis), i.e., $\delta/\lambda_0 = 0.12$, about at the peak of the efficiency curve, as pointed out in Fig. 8. Even if a slightly higher efficiency could be achieved at a shorter distance, we stayed to the right-hand side of the peak in order to avoid falling (due to changes in loading conditions) into the steep region to its left-hand side where the efficiency drops sharply.

The broad-band tuning capability of the exciter has been demonstrated using the optimized radial cavity, and the measured return loss is displayed in Fig. 9. Comparing Figs. 6 and 9, we notice that the matching to the source is not as good for the radial cavity as it was for the terminated waveguide. The amount of power dissipated (as well as radiated) at 900 MHz is very close to the prediction, hinting that a relatively low percentage of power is bounced back into the cavity when the reflected wave impinges on the input port. As it will be shown later, measurements show that the fraction of RF power radiated is minimal. The power lost in the metal and plastics is low as well, meaning that the great majority of it is dissipated in the mice.

IV. Determination of the Whole-Body Average SAR

The whole-body SAR in the mice is found by dividing the power dissipated in the animals by their mass, thus, it is important to determine this power precisely. The power balance

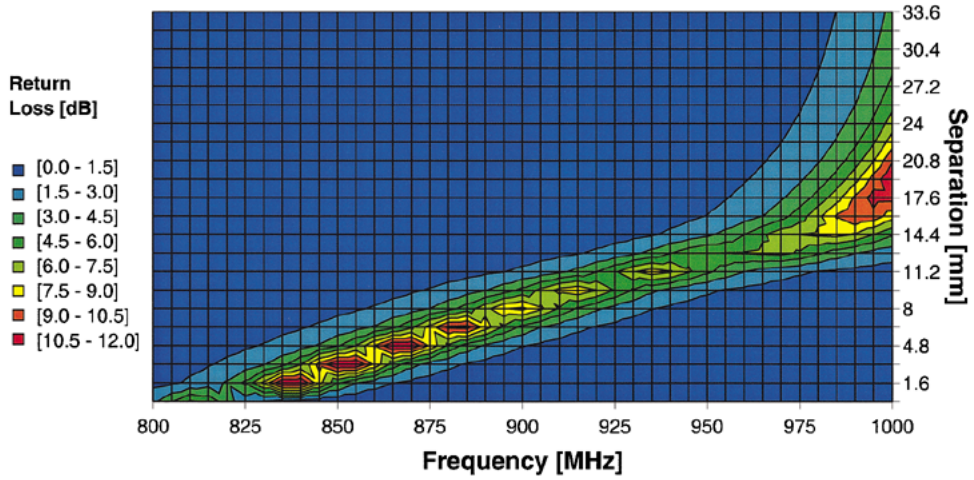

Fig. 9. Return loss of the "Ferris wheel," achieved by using the tunable exciter to optimize the impedance match to the 50-Ω feed line.

equation—$P_{\text{mice}} = (P_{\text{inc}} - P_{\text{ref}}) - (P_{\Omega} + P_{\text{rad}})$—states that the power dissipated in the mice can be found by measuring the incident (P_{inc}) and reflected (P_{ref}) power at the cavity port, and estimating the ohmic losses in metal and dielectric losses in plastics (P_{Ω}) and the radiated power (P_{rad}). The first two contributions are measurable throughout the exposure using a bidirectional coupler. The ohmic and dielectric losses have been estimated measuring the return loss and the power radiated by the unloaded cavity at 900 MHz, the missing power accounting for about 1% of the incident power. Determination of the radiated power is described below.

A. RF Leakage

The cylindrical symmetry of the radiation pattern simplifies RF leakage measurements drastically since it allows determining the total amount of radiated power by measuring a single elevation cut. This symmetry is preserved even though the cylindrical symmetry of the cavity is compromised by the 40 circular holes on each plate and by the array of shorting posts. The reason is twofold. First, the distance between holes (about 8 cm center-to-center) is smaller than a half-wavelength at 900 MHz (the distance between posts is three times shorter and, therefore, negligible in this context). Second, the circular distribution of the radiating slots mitigates the effect of phase-delay differences to the observation point. This has been verified by measuring the H-plane ($z = 0$) radiation pattern of the cavity prototype. Using a simple model comprising 40 equidistant half-wave dipoles forming a circular array 1 m in diameter, it can be seen that the azimuth pattern is practically flat, its fluctuation staying below 1% up to 2.7 GHz. This frequency range includes the 1.8–1.9- and 2.45-GHz bands, which host other wireless services, that are likely to be addressed in future studies. Finally, for a fixed operating frequency, a limitation in size may be established, which would translate in a corresponding limitation in the number of animals sharing the exposure unit.

As previously remarked, 120 shorting posts placed at 48 cm from the center have been used instead of a solid lateral wall for the "Ferris wheel" cavity to provide light to the exposed mice, thus limiting the stress induced on these animals. We have

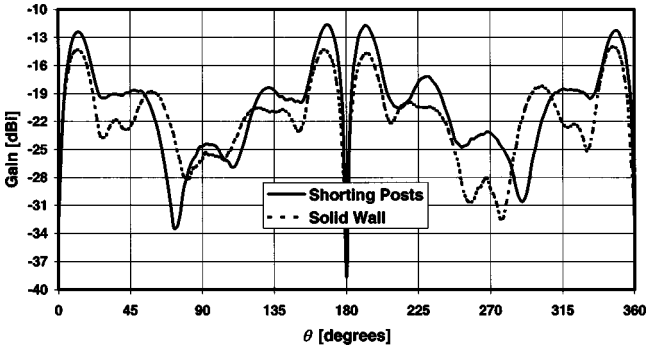

(a)

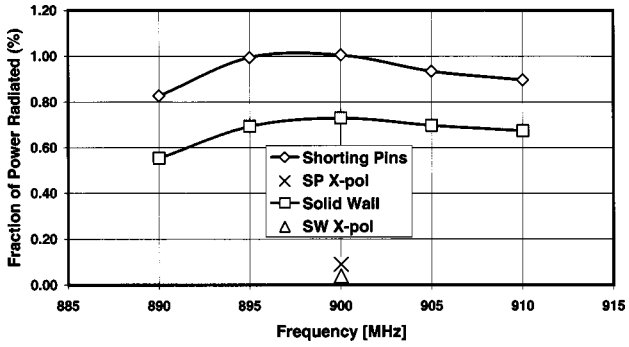

(b)

Fig. 10. Comparison of the radiation characteristics of the "Ferris wheel" with shorting posts or a solid lateral wall. (a) Measured radiation pattern over an elevation cut at 900 MHz. (b) Fraction of the incident RF power that is radiated (the cross polarization was measured only at 900 MHz).

studied the effect of this solution on the RF leakage by comparing the radiated power by the loaded cavity in the case of a solid wall versus using shorting posts. In Fig. 10(a), the measured elevation cuts (constant ϕ) at 900 MHz for the "Ferris wheel" with a solid lateral wall or the shorting posts are reported. In Fig. 10(b), the measured fraction of power radiated in the two cases is compared at several frequencies, showing the relatively large increase in the case of the discontinuous wall. This indicates that about 30% of the radiated power is leaked from the array of shorting posts, while the rest is attributable to the circular slots. Also, the radiated power associated to the spurious cross-polarized field (ϕ-component) is shown to be negli-

gible. In absolute terms, the fraction of radiated power is very small (≈1%) due to the low efficiency of the radiating apertures since the distance between posts (about 2.5 cm) is much smaller than the wavelength at this frequency, and E_ϕ is weakly excited [as shown by the low levels of cross-polarized radiation in Fig. 10(b)].

Given the limited loss of energy to ohmic effects and radiation, it can be assumed that these losses do not vary significantly over relatively wide changes of the loading conditions. Therefore, the amount of power dissipated in the mice can be determined just by monitoring bidirectional power flow, so that the collective whole-body average SAR is

$$\mathrm{SAR}_{WB} = \frac{P_{\mathrm{mice}}}{m_{\mathrm{mice}}} = \frac{P_{\mathrm{inc}} - P_{\mathrm{ref}} - (\alpha_\Omega + \alpha_{\mathrm{rad}})P_{\mathrm{inc}}}{m_{\mathrm{mice}}} \quad (6)$$

where $\alpha_\Omega \approx 0.01$, $\alpha_{\mathrm{rad}} \approx 0.01$, and m_{mice} is the total mass of the 40 animals. Such a determination of the SAR is quite accurate since it mainly relies on power measurements. The assumption here is that the dissipated RF power is equally spread among mice, which may not be the case if some of them grow in body size abnormally. Typically, over the duration of a long-term study, the mice are weighed on a weekly basis, so the history of the exposure can be compiled accurately by combining this information with the monitored power data.

We performed thermometric measurements to verify the accuracy of (6). In this case, the experimental setup comprises the "Ferris wheel" loaded with dummy equivalents. One of the dummies is encapsulated in a Styrofoam shell where a small hole allows the insertion of a Vitek-101 thermistor probe, which is substantially transparent (nonperturbing) to the electromagnetic field, to sense the temperature. A short high-power RF exposure (30 W for 2 min) induces a temperature rise in the dummy. The dummy is vigorously shaken after exposure to equalize the temperature throughout, thus, the correct average temperature increase reading can be taken regardless of the actual position of the thermistor inside the dummy. Provided the heat exchange with the external environment is negligible because of the Styrofoam enclosure, the difference between the final and initial average temperature in the dummy is proportional to the dissipated RF power, therefore,

$$\mathrm{SAR}_{\mathrm{dummy}} = \frac{W_{\mathrm{dummy}}}{m_{\mathrm{dummy}}} = c_{\mathrm{dummy}} \frac{\overline{T}_f - \overline{T}_i}{\Delta t} \quad (7)$$

where W_{dummy} is the average time rate of RF energy deposition in the dummy, m_{dummy} is its mass, $c_{\mathrm{dummy}} \approx 2.8 \pm 0.1$ J/g · K is the specific heat of the particular tissue-equivalent solution that was employed, and Δt is the exposure duration. The whole-body average SAR in the mice is found by taking into account the difference in density

$$\mathrm{SAR}_{WB} = \mathrm{SAR}_{\mathrm{dummy}} \frac{\rho_{\mathrm{dummy}}}{\rho_{\mathrm{mice}}} \quad (8)$$

where $\rho_{\mathrm{dummy}} \approx 1.25$ g/cm^3, and $\rho_{\mathrm{mice}} \approx 1$ g/cm^3. Fig. 11 shows details of the experimental setup, while Fig. 12 reports the results of ten thermal measurements performed on dummy equivalents, given in terms of the fraction of the incident power

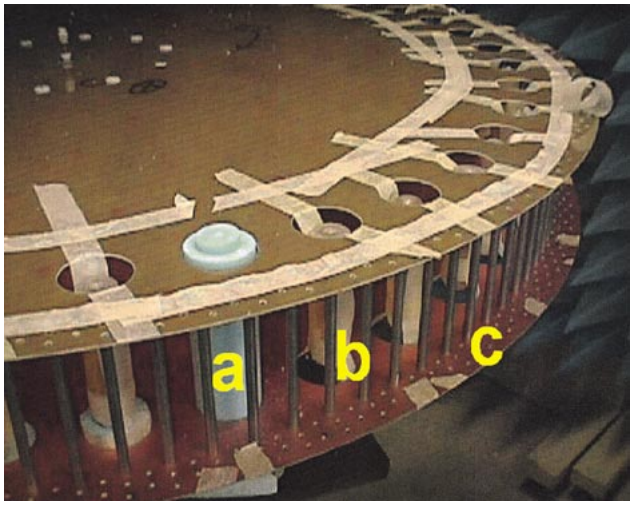

Fig. 11. Experimental setup used to perform thermal SAR measurements in order to verify the estimate provided by (6). The dummy under test is encapsulated in: (a) a Styrofoam shell, while (b) the others are suspended by means of masking tape. (c) Different hole patterns used to optimize the cavity efficiency by varying the distance of the shorting-post array are also visible.

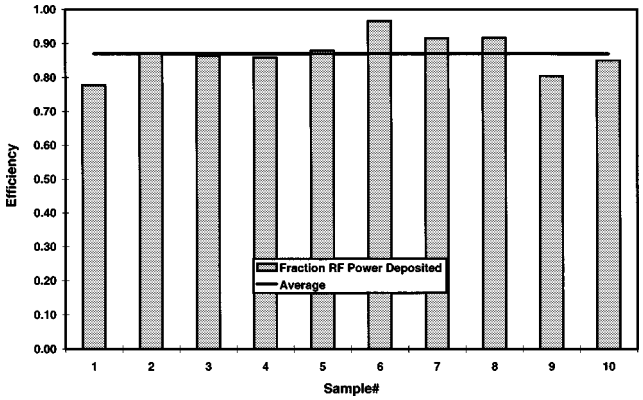

Fig. 12. Fraction of the incident RF power that is dissipated in the mice, obtained by means of thermal SAR measurements performed on 30-g dummy equivalents.

that is absorbed in the dummy. These results also illustrate the dispersion of whole-body SAR values. Further efforts, which will be documented in a separate paper, have been devoted to perform a complete dosimetric study, which included using calorimetric techniques to measure whole-body RF absorption, as well as determining the SAR distribution in the mice by means of thermographic measurements and computations. This study shows improved uniformity of the SAR distribution with respect to typical plane-wave incidence, due to the animals' exposure to the waves reflected by the lateral cavity wall.

During the course of a two-year bioassay and particularly toward the end, a certain number of animals will die. When that happens, they are replaced with dummy equivalents in order to preserve the symmetrical energy distribution during exposure.

V. Remarks

In long-term animal bioassays, it is extremely important to isolate the agent whose effect one wants to study. Consequently, a well-designed study should point out potential confounding factors and remove them. These factors include physical agents

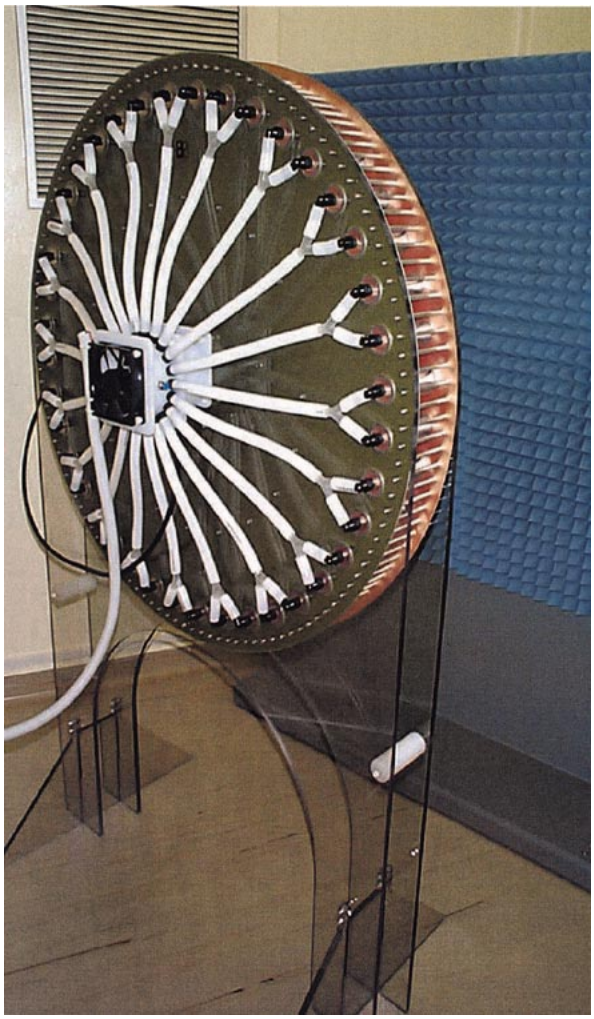

Fig. 13. Details of the airflow system implemented on the units employed at the IMVS, Adelaide, South Australia. The dc fan pushes air, which is distributed to the mice through hoses departing from the air plenum. Pressure in the plenum is constantly monitored.

(e.g., chemical or biological carcinogenic agents, acoustic noise, thermal stress, undesired electromagnetic-field sources, etc.). We totally avoided the use of glues to assemble the exposure systems. The airflow system shown in Fig. 13 uses bio-compatible rubber tubing for medical applications (C-FLEX, Cole-Parmer), and features a pressure sensor to detect inadvertent flow stoppage. We also verified that the static and low-frequency magnetic fields generated by the airflow fan would be negligible at the location where the mice were to be exposed, opting for a dc fan over ac fans to reduce as much as possible the magnetic-field intensity. At the Australian exposure facility, the acoustic noise coming from the cooling fans of the RF equipment, as well as from the airflow fan, was measured and actions were taken to reduce it where appropriate. The airflow at the facility itself is filtered to avoid contamination from external agents, and the high rate of air recycle limits potential effects of outgassing of substances from the materials (plastics, RF absorbers, etc.) inside the exposure rooms. Engineering expertise *per se* is not sufficient to address many of the issues just mentioned, which is why the inputs and constant feedback from the biologists that conduct the bioassay is fundamental to proceed successfully in the design.

Likely, the "Ferris wheel" could be adopted to perform other studies in the future. Some of these studies may be carried out at other frequencies and with different RF signals. Whereas the effect of the linear distortion caused by the frequency response characteristics of the cavity should not degrade the modulation of the RF signals, unless we are dealing with signals having extremely wide fractional bandwidths, more serious effects could derive from the cavity overmoding at the higher frequencies. For instance, at 1.8 GHz, the present dimensions of the "Ferris wheel" determine the excitation of radially propagating modes with z-variation. Mode filters could be needed to reestablish the TEM wave in order to maintain the most uniform exposure of the mice, as well as to reduce the radiation efficiency of the apertures.

VI. Conclusions

The "Ferris-wheel" exposure system has been designed with the intent of providing an efficient means for conducting large-scale long-term animal studies of whole-body RF exposure. Remarkable savings in terms of space and RF equipment cost have resulted from the implementation of a closed electromagnetic structure. One of the key features of this structure is the tunability across a wide frequency band, as well as loading conditions, without resorting to external matching circuits. The modest amount of radiated power has a twofold benefit: it allows determining the whole-body average SAR by means of simple and accurate bidirectional power measurements and it allows to place several units in close proximity to each other with minimal RF screening to preserve mutual isolation. The high number of animals that can be exposed simultaneously in a single unit allows substantial savings in terms of the laboratory area needed to carry out the study. The "Ferris wheel" has a remarkably high efficiency so that the cost (tightly related to the budgeted RF power) to carry out large-scale bioassays is drastically reduced with respect to the case where electromagnetically open exposure systems are employed. As a matter of fact, with a minimal amount of redesign, the "Ferris wheel" could be the first exemplar of a family of exposure systems to be employed in several upcoming bioassays.

Appendix

The electromagnetic-field distribution in a radial waveguide is derived, assuming no vertical variation $(\partial/\partial z = 0)$, as well as perfect metal conductors. These hypotheses yield $\mathbf{E}_t = \hat{\rho}E_\rho + \hat{\phi}E_\phi = \mathbf{0}$. Consequently, $\nabla \cdot \mathbf{E} = 0$ within the field domain. If we assume that the impressed current is uniformly distributed on a vertical cylinder of radius a

$$\mathbf{J} = \hat{\mathbf{z}}\,\frac{I_0}{2\pi a}\,\delta(\rho - a), \qquad 0 \le z \le h \tag{A1}$$

the Maxwell's equations yield

$$\nabla_t^2 E_z + k^2 E_z = j\omega\mu\,\frac{I_0}{2\pi a}\,\delta(\rho - a), \qquad 0 \le z \le h. \tag{A2}$$

with $k^2 = -j\omega\mu(\sigma + j\omega\varepsilon)$, σ being the dielectric conductivity. Due to the cylindrical symmetry of the structure and the source,

the electromagnetic-field components depend only on the radial variable ρ. The boundary condition of E_z on the source is obtained by integrating (A2) over the surface $\rho' \leq \rho$ as $\rho \to a$, resulting

$$\lim_{\rho \to a} 2\pi\rho \frac{\partial E_z}{\partial \rho} = j\omega\mu I_0. \tag{A3}$$

The solution of (A2) subject to (A3) is well known [15]

$$E_z(\rho) = A_r H_0^{(1)}(k\rho) + A_f H_0^{(2)}(k\rho) \tag{A4}$$

where $H_0^{(1)}$, $H_0^{(2)}$ are zeroth-order Hankel functions that, respectively, describe inward and outward cylindrical waves. The magnetic field is simply derived as $\mathbf{H} = -\nabla \times \mathbf{E}/j\omega\mu$, thus, its only component is expressed in terms of Hankel functions of the first order

$$H_\phi(\rho) = \frac{1}{j\omega\mu} \frac{\partial E_z}{\partial \rho} = \frac{1}{-j\eta} \left[A_r H_1^{(1)}(k\rho) + A_f H_1^{(2)}(k\rho) \right] \tag{A5}$$

where $\eta = \sqrt{j\omega\mu/(\sigma + j\omega\varepsilon)}$ is the wave impedance in the medium. The complex power generated by the source is found applying Poynting's theorem

$$\begin{aligned} P_g &= \frac{1}{2} \oint_S \mathbf{E} \times \mathbf{H}^* \cdot \hat{\rho}\, dS \\ &= -\frac{1}{2} \int_V \mathbf{E} \cdot \mathbf{J}^*\, dV \\ &= -\frac{1}{2} E_z(a) I_0^* h. \end{aligned} \tag{A6}$$

where the symbol * represents the conjugate complex operator. Equation (A6) does not allow to discriminate between forward- and reverse-power flow. These contributions are

$$\begin{aligned} P_f &= \frac{1}{2}\mathrm{Re} \int_0^h dz \int_0^{2\pi} \hat{\rho} \\ &\quad \cdot \left[\hat{\mathbf{z}} A_f H_0^{(2)}(k\rho) \times \hat{\phi} A_f^* \frac{H_1^{(2)}(k\rho)^*}{j\eta^*} \right] \rho\, d\phi \\ &= -\frac{1}{2} 2\pi\rho |A_f|^2 h \mathrm{Re} \left\{ \frac{H_0^{(2)}(k\rho) H_1^{(2)}(k\rho)^*}{j\eta^*} \right\} \end{aligned} \tag{A7a}$$

$$\begin{aligned} P_r &= \frac{1}{2}\mathrm{Re} \int_0^h dz \int_0^{2\pi} (-\hat{\rho}) \\ &\quad \cdot \left[\hat{\mathbf{z}} A_r H_0^{(1)}(k\rho) \times \hat{\phi} A_r^* \frac{H_1^{(1)}(k\rho)^*}{j\eta^*} \right] \rho\, d\phi \\ &= \frac{1}{2} 2\pi\rho |A_r|^2 h \mathrm{Re} \left\{ \frac{H_0^{(1)}(k\rho) H_1^{(1)}(k\rho)^*}{j\eta^*} \right\}. \end{aligned} \tag{A7b}$$

Evidently, for $\rho \to a$, we must find $P_f - P_r = \mathrm{Re}\{P_g\}$, which holds as long as no losses occur at any distance shorter than ρ.

ACKNOWLEDGMENT

The authors gratefully acknowledge the support of the entire staff at the Motorola Florida Electromagnetics Research Laboratory, Fort Lauderdale, FL, and especially the contributions of M. Ballen, M. Kanda, and Dr. J. Morrissey, Dr. M. Swicord, as well as the guidance of Dr. T. Kuchel and Dr. T. Utteridge, IMVS, Adelaide, South Australia.

REFERENCES

[1] J. A. D'Andrea, J. R. DeWitt, O. P. Gandhi, S. Stensaas, J. L. Lords, and H. C. Nielson, "Behavioral and physiological effects of chronic 2,450-MHz microwave irradiation of the rat at 0.5 mW/cm^2," *Bioelectromagnetics*, vol. 7, no. 1, pp. 45–56, 1986.

[2] C. K. Chou, A. W. Guy, L. L. Kunz, R. B. Johnson, J. Crowley, and J. H. Krupp, "Long-term, low-level, microwave irradiation of rats," *Bioelectromagnetics*, vol. 13, no. 6, pp. 469–496, 1992.

[3] M. H. Repacholi, A. Basten, V. Gebski, D. Noonan, J. Finnie, and A. W. Harris, "Lymphomas in Eμ-Pim1 transgenic mice exposed to pulsed 900 MHz electromagnetic fields," *Radiat. Res.*, vol. 147, pp. 631–640, 1997.

[4] J. C. Toler, W. W. Shelton, M. R. Frei, J. H. Merritt, and M. A. Stedham, "Long-term, low-level exposure of mice prone to mammary tumors to 435 MHz radiofrequency radiation," *Radiat. Res.*, vol. 148, no. 3, pp. 227–234, 1997.

[5] M. R. Frei, R. E. Berger, S. J. Dusch, V. Guel, J. R. Jauchem, J. H. Merritt, and M. A. Stedham, "Chronic exposure of cancer-prone mice to low-level 2450 MHz radiofrequency radiation," *Bioelectromagnetics*, vol. 19, no. 1, pp. 20–31, 1998.

[6] W. R. Adey, C. V. Byus, C. D. Cain, R. J. Higgins, R. A. Jones, C. J. Kean, N. Kuster, A. MacMurray, R. B. Stagg, G. Zimmerman, J. L. Phillips, and W. Haggren, "Spontaneous and *nitrosourea*-induced primary tumors of the central nervous system in Fischer 344 rats chronically exposed to 836 MHz modulated microwaves," *Radiat. Res.*, vol. 152, no. 3, pp. 293–302, 1999.

[7] C. K. Chou, H. Bassen, J. Osepchuk, Q. Balzano, R. Petersen, M. Meltz, R. Cleveland, J. C. Lin, and L. Heynick, "Radio frequency electromagnetic exposure: Tutorial review on experimental dosimetry," *Bioelectromagnetics*, vol. 17, no. 3, pp. 195–208, 1996.

[8] International Commission on Non-Ionizing Radiation Protection (ICNIRP), "Guideline for limiting exposure to time-varying electric, magnetic, and electromagnetic fields," *Health Phys.*, vol. 74, no. 4, pp. 494–522, Apr. 1998.

[9] *Standard for Safety Levels with Respect to Human Exposure to RF Electromagnetic Fields, 3 kHz to 300 GHz*, IEEE/ANSI Standard C95.1-1992, 1999.

[10] A. W. Guy, "Miniature anechoic chamber for chronic exposure of small animals to plane-wave microwave fields," *J. Microwave Power*, vol. 14, no. 4, pp. 327–338, 1979.

[11] C. K. Chou and A. W. Guy, "Systems for exposing mice to 2,450-MHz electromagnetic fields," *Bioelectromagnetics*, vol. 3, no. 4, pp. 401–412, 1982.

[12] S. Bonasera, J. Toler, and V. Popovic, "Long-term study of 435 MHz radio-frequency radiation on blood-borne end points in cannulated rats. Part I: Engineering considerations," *J. Microwave Power Electromag. Energy*, vol. 23, no. 2, pp. 95–104, 1988.

[13] V. W. Hansen, A. K. Bitz, and J. R. Streckert, "RF exposure of biological systems in radial waveguides," *IEEE Trans. Electromagn. Compat.*, vol. 41, pp. 487–493, Nov. 1999.

[14] C. K. Chou, "State of the science regarding *in vitro* and *in vivo* exposure systems for RF studies," in *Wireless Phones and Health—Scientific Progress*, G. Carlo, Ed. Norwell, MA: Kluwer, 1998, ch. 1.

[15] S. Ramo, J. R. Whinnery, and T. Van Duzer, *Fields and Waves in Communication Electronics*. New York: Wiley, 1965, ch. 9.

[16] G. Hartsgrove, A. Kraszewski, and A. Surowiec, "Simulated biological materials for electromagnetic radiation absorption studies," *Bioelectromagnetics*, vol. 8, no. 1, pp. 29–36, 1987.

[17] R. Collin, *Antennas and Radio Wave Propagation*. New York: McGraw-Hill, 1985.

Quirino Balzano (S'63–M'72–SM'83) was born in Rome, Italy, in December 1940. He received the Doctorate in Engineering degree in electronics from the University of Rome, Rome, Italy, in 1965.

During 1966, he was with FIAT, S.p.A., Turin, Italy. From 1967 to 1974, he was with the Missile Systems Division, Raytheon Corporation, where he was involved in the research and development of planar and conformal phased arrays. Since 1974, he has been with Motorola Inc., Plantation, FL, where he is the Corporate Vice President and Director of the Motorola Florida Research Laboratories, Fort Lauderdale, FL. His main interest is in the biological effects of human exposure to RF electromagnetic energy. He has authored or co–authored over 50 papers in RF dosimetry near electromagnetic sources and the biological effects of RF energy. He holds 27 patents in antenna and integrated-circuit (IC) technology, He was on the Board of Directors of the Bioelectromagnetics Society, a scientific society dedicated to the research of the biological effects of electromagnetic fields.

Dr. Balzano was the recipient of the 1978 and 1982 IEEE Vehicular Technology Society Paper Prize Award and a 1981 Certificate of Merit presented by the Radiological Society of North America for the treatment of tumors with RF energy.

Chung-Kwang Chou (S'72–M'75–SM'86–F'89) was born in Chung-King, China, on May 11, 1947. He received the B.S. degree from the National Taiwan University, Taipei, R.O.C., in 1968, the M.S. degree from Washington University, St. Louis, MO, in 1971, and the Ph.D. degree from the University of Washington, Seattle, in 1975, all in electrical engineering.

After spending a year as a National Institutes of Health Post-Doctoral Fellow in the Regional Primate Research Center and the Department of Physiology and Biophysics at the University of Washington, he served as Assistant Professor from 1977 to 1981 and Research Associate Professor from 1981 to 1985 in the Department of Rehabilitation Medicine and Center for Bioengineering, University of Washington. From 1985 to 1998, he was a Research Scientist and the Director of the Department of Radiation Research at the City of Hope National Medical Center, Duarte, CA. Since April 1998, he has been the Director of the Corporate RF Dosimetry Laboratory, Motorola Florida Research Laboratories, Fort Lauderdale, FL. He has authored or co-authored 150 papers and book chapters. His research has been on RF biological effects, RF dosimetry and exposure systems, hyperthermia, and electrochemical treatment of cancer. His professional service include member of the Board of Directors of the Bioelectromagnetics Society (1981–1984), Associate Editor of the *Journal of Bioelectromagnetics* (1987–present), for which he is responsible for editing papers on high-frequency RF fields, the Electromagnetics Academy (1990–present), Vice Chairman of Committee 89-5 on "Biological effects and exposure criteria for radio frequency electromagnetic fields" of the National Council on Radiation Protection and Measurements (1996–present), and Council Member of the NCRP (1998–2004).

Dr. Chou is a member of BEMS, Tau Beta Pi and Sigma Xi, and is a Fellow of the American Institute for Medical and Biological Engineering. He has been the chairman of the IEEE/EMBS Committee on Man and Radiation (1996–1997), and is co-chairman of the IEEE Scientific Coordinating Committee 28, Subcommittee 4 on RF safety Standard (1997–present). He was the recipient of the first special award for the decade (1970–1979) presented by the International Microwave Power Institute in 1981, the 1985 Outstanding Paper Award presented by the *Journal of Microwave Power*, and the 1995 Curtis Carl Johnson Memorial Award for Preceptor of Best Student Poster presented by the Bioelectromagnetics Society. He was also a Distinguished Lecturer of the IEEE Engineering in Medicine and Biology Society (1991–1992).

Renato Cicchetti (S'83–M'83) was born in Rieti, Italy, in 1957. He received the Laurea degree (*cum laude*) in electronic engineering from the University of Rome "La Sapienza," Rome, Italy, in 1983.

From 1983 to 1986, he was an Antenna Designer at Selenia Spazio S.p.A. (now Alenia Aerospazio S.p.A.), Rome, Italy, where he was involved in studies on theoretical and practical aspects of antennas for space application and scattering problems. Since 1986, he has been a Researcher in the Dipartimento di Elettronica, University of Rome "La Sapienza," where he is currently an Associate Professor. In 1998, he was Visiting Professor at the Motorola Florida Corporate Electromagnetics Research Laboratory, Fort Lauderdale, FL, where he was involved with antennas for cellular communications. He also serves as a Reviewer of several scientific journals. His current research interests include electromagnetic-field theory, asymptotic techniques, electromagnetic compatibility, wireless communications, microwave and millimeter-wave integrated circuits, and antennas. He is listed in *Who's Who in the World* and *Who's Who in Science and Engineering*.

Dr. Renato Cicchetti is a member of the Italian Electrical and Electronic Society (AEI).

Antonio Faraone (M'97) was born in Rome, Italy, in April 1966. He received the Laurea degree (*magna cum laude*) in electronics engineering and the Ph.D. degree in applied electromagnetics from the University of Rome "La Sapienza," Rome, Italy, in 1992 and 1997, respectively.

Since 1997, he has been with the Motorola Florida Research Laboatories, Fort Lauderdale, FL, where he is the Manager of Antenna Research, involved in theoretical and experimental research in antenna technology RF dosimetry. He holds four patents. His research interests further include electromagnetic compatibility (EMC) and full-wave modeling. He is a member of the International Union of Radio Science (URSI) and serves as a reviewer for several scientific journals.

Dr. Faraone received the 1993 Giorgio Barzilai Prize presented by the IEEE Central and South Italy Section for his Laurea dissertation.

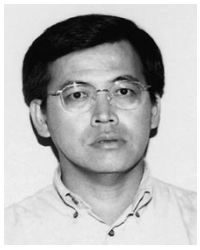

Roger Yew-Siow Tay (S'82–M'86) was born in Johor Baru, Malaysia, in 1958. He received the B.S. and M.S. degrees in electrical engineering from the University of Massachusetts, Lowell, in 1983 and 1985, respectively, and the Ph.D. degree from the Swiss Federal Institute of Technology (ETH), Zurich, Switzerland, in 1997.

In 1987, he returned to the Far East and joined the Research and Development Department, Motorola Electronics Pte. Ltd., Singapore. In 1990, he joined the Florida Electromagnetics Laboratory, Motorola Inc, Fort Lauderdale, FL. In 1993, he was and Invited Academic Guest to the ETH for eight months. Following this, he returned to the Motorola Corporate Electromagnetics Research Laboratory, Fort Lauderdale, FL, as Principal Staff Engineer. In 1998, he returned to the Singapore Design Center, Motorola Electronics Pte. Ltd., Singapore, as Senior Principal Staff Engineer, where he set up the Electromagnetics Laboratory within the Singapore Design Center. He has authored or co-authored many papers in journals and conferences. He holds six patents with four pending.

Dr. Tay is a member of the IEEE Antennas and Propagation Society and the IEEE Electromagnetics Compatibility Society.